3D Scaffolds with Different Stiffness but the Same Microstructure for Bone Tissue Engineering
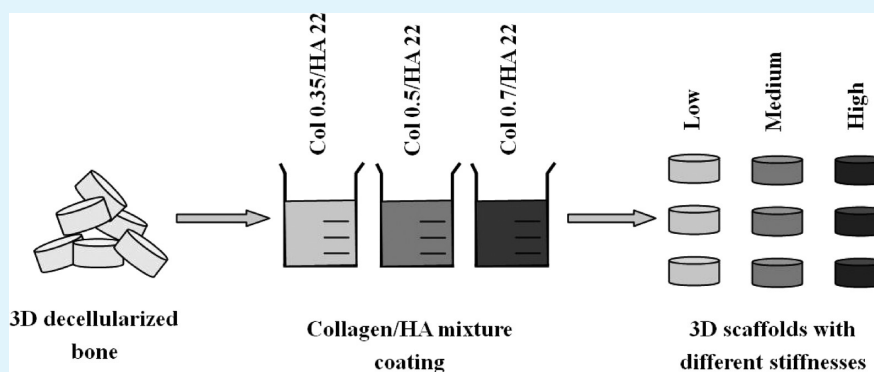
Guobao Chen,[†,‡] Chanjuan Dong,[†,‡] Li Yang,[†,‡] and Yonggang Lv*[,†,‡]

[†]Key Laboratory of Biorheological Science and Technology (Chongqing University), Ministry of Education, and [‡]'111' Project Laboratory of Biomechanics and Tissue Repair, Bioengineering College, Chongqing University, Chongqing 400044, P. R. China

S *Supporting Information*

ABSTRACT: A growing body of evidence has shown that extracellular matrix (ECM) stiffness can modulate stem cell adhesion, proliferation, migration, differentiation, and signaling. Stem cells can feel and respond sensitively to the mechanical microenvironment of the ECM. However, most studies have focused on classical two-dimensional (2D) or quasi-three-dimensional environments, which cannot represent the real situation *in vivo*. Furthermore, most of the current methods used to generate different mechanical properties invariably change the fundamental structural properties of the scaffolds (such as morphology, porosity, pore size, and pore interconnectivity). In this study, we have developed novel three-dimensional (3D) scaffolds with different degrees of stiffness but the same 3D microstructure that was maintained by using decellularized cancellous bone. Mixtures of collagen and hydroxyapatite [HA: $Ca_{10}(PO_4)_6(OH)_2$] with different proportions were coated on decellularized cancellous bone to vary the stiffness (local stiffness, 13.00 ± 5.55 kPa, 13.87 ± 1.51 kPa, and 37.7 ± 19.6 kPa; bulk stiffness, 6.74 ± 1.16 kPa, 8.82 ± 2.12 kPa, and 23.61 ± 8.06 kPa). Microcomputed tomography (μ-CT) assay proved that there was no statistically significant difference in the architecture of the scaffolds before or after coating. Cell viability, osteogenic differentiation, cell recruitment, and angiogenesis were determined to characterize the scaffolds and evaluate their biological responses *in vitro* and *in vivo*. The *in vitro* results indicate that the scaffolds developed in this study could sustain adhesion and growth of rat mesenchymal stem cells (MSCs) and promote their osteogenic differentiation. The *in vivo* results further demonstrated that these scaffolds could help to recruit MSCs from subcutaneous tissue, induce them to differentiate into osteoblasts, and provide the 3D environment for angiogenesis. These findings showed that the method we developed can build scaffolds with tunable mechanical properties almost without variation in 3D microstructure. These preparations not only can provide a cell-free scaffold with optimal matrix stiffness to enhance osteogenic differentiation, cell recruitment, and angiogenesis in bone tissue engineering but also have significant implications for studies on the effects of matrix stiffness on stem cell differentiation in 3D environments.

KEYWORDS: *bone tissue engineering, 3D microenvironment, osteogenic differentiation, mesenchymal stem cells, matrix stiffness, decellularized cancellous bone*

1. INTRODUCTION

Different tissues have well-defined elastic moduli ranging from very soft tissues, such as the brain ($\sim$1 kPa), to stiffer tissues like skeletal muscle ($\sim$10 kPa), and the even higher rigidity found in bone tissue ($\sim$15 MPa).[1,2] Matrix mechanics have been proven to be an important regulator for cellular behavior and function, including cell adhesion, proliferation, migration, and differentiation.[3–7] Engler et al.[8] have demonstrated that human mesenchymal stem cells (MSCs) can differentiate into neurons, myoblasts, or osteoblasts when they are cultured on collagen-coated polyacrylamide (PA) hydrogels with stiffness similar to that of the brain (0.1–1 kPa), muscle (8–17 kPa), or collagenous bone
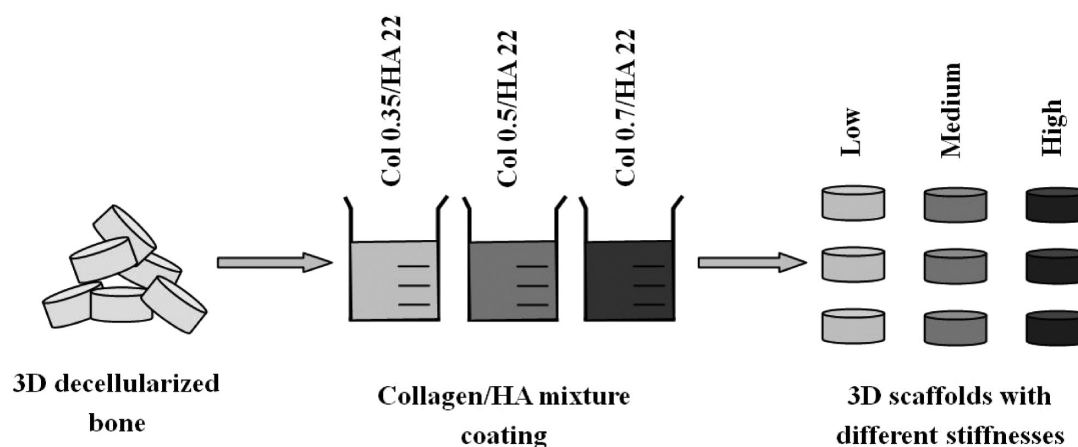
Figure 1. Schematic diagram of the fabrication process of 3D scaffolds with different stiffness. Decellularized cancellous bone was used to maintain the same 3D microstructure. Different proportions of collagen/HA mixtures were coated on the decellularized cancellous bone to form different stiffness values.

(25−40 kPa). Recently, Yang et al.[9] also found that a one-week culture of MSCs on rigid surfaces (10 kPa) promotes nuclear runx2 expression that remains active after the surrounding matrix is softened. MSCs can store the information from past physical environments and influence the cells' fate. This finding is consistent with a recent report by Lee and colleagues,[10] who demonstrated that MSCs remain susceptible to the biophysical properties of the matrix and can redirect lineage specification in response to changes in the microenvironment even after several weeks of culture. It has also been shown that the stiffness of the adhesion matrix for MSCs can adjust the differentiation effects of growth factors such as transforming growth factor-β (TGF-β) or vascular endothelial growth factor (VEGF).[11,12] However, most previous studies on the effects of matrix stiffness on cell behavior and function were performed on classical 2D or a quasi-three-dimensional environment, which cannot represent the real situation *in vivo*. The biochemistry, topology, and mechanical properties in real three-dimensional (3D) microenvironments are much different from those in the conventional 2D condition.[13,14] Most cells require cues from a truly 3D environment to form relevant physiological tissues and organs in the body.[15]

In recent studies, changing the matrix density of natural proteins in different positions,[16] using synthetic polymers with tunable cross-linking densities,[17,18] and changing the ratios of mixed matrices with varied elasticity[19,20] have been used to generate 3D scaffolds with different mechanical properties. However, these methods invariably change the fundamental structural properties of the 3D scaffolds (such as morphology, porosity, pore size, and pore interconnectivity) at the same time. Recently, Huebsch et al.[21] fabricated a model matrix with different stiffness by engineering a synthetic hydrogel extracellular matrix (ECM) to examine the commitment of the clonally derived murine MSCs in 3D microenvironments with different rigidities (2.5−110 kPa). They found that the osteogenic commitment occurred predominantly at 11−30 kPa. It is still a major challenge to build scaffolds with the same 3D microstructure but different degrees of stiffness. The key issue facing 3D matrix mechanics research is how to build a material that has tunable mechanical properties while maintaining the same 3D microstructure.

In order to meet this challenge, decellularized cancellous bone was used in this study to maintain the 3D microstructure of the scaffold. Mixtures of collagen and hydroxyapatite [HA, $Ca_{10}(PO_4)_6(OH)_2$] with different proportions were coated on the decellularized cancellous bone scaffolds, which can provide different degrees of stiffness on the surface of the scaffolds after lyophilization (Figure 1). Decellularized tissue has the same structure and composition as natural tissue and has been thought to be an appropriate material for a 3D scaffold to provide a desirable cellular microenvironment for several kinds of stem cells.[22,23] HA was used in our study due to its high biocompatibility and close similarity in chemical composition with natural bone tissue. Because of the poor mechanical property of the pure HA scaffold, HA was mixed with collagen solution. As an important component of bone, collagen has good biocompatibility, low immunogenicity, proper osteoinductive function,[24] and complete biodegradability. In addition, collagen can protect and support human tissue and the physical property of bone.[25] There is evidence that a collagen and HA mixture has appropriate mechanical properties for bone repair and that the proportion of collagen in the mixed material plays an important role in determining the mechanical property of the collagen/HA matrix. For instance, the Young's modulus of elasticity (E) of the material changes from 62.02 to 289.98 kPa when the proportion of collagen changes from 0.5% to 2%, while the proportion of HA is maintained at the same 50%.[26] Furthermore, collagen/HA coating incorporated into decellularized cancellous bone is expected to modulate the surrounding biological environment to further facilitate osseointegration and mitigate possible adverse tissue responses, including foreign body reaction and implant infection. In this study, 3D scaffolds with different stiffness while having the same 3D microstructures were first prepared. Then, the biological responses of these scaffolds *in vitro* and *in vivo* were evaluated in terms of cell viability, osteogenic differentiation, cell recruitment, and angiogenesis.

2. MATERIALS AND METHODS

2.1. Isolation and Culture of Rat MSCs. Primary rat MSCs were isolated from the tibias and femurs of 4-week-old Sprague−Dawley (SD) rats weighing 130 ± 10 g (Animal Center, Daping Hospital, Third Military Medical University, Chongqing, China) as described previously.[27] All animal experimental procedures were carried out according to the protocols approved by Chongqing University Animal Care and Use Committee. MSCs were isolated by Percoll density gradient centrifugation (1.073 g/L) and grown at 37 °C and 5% CO_2
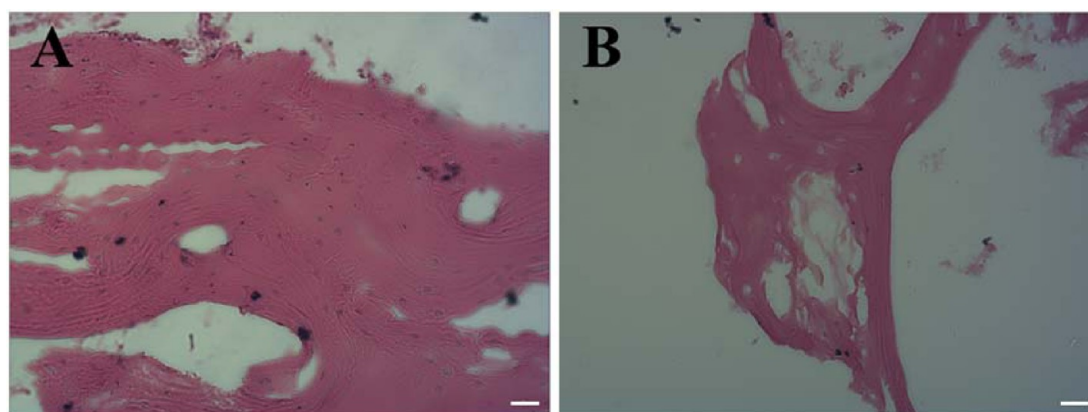
Figure 2. H-E staining of native cancellous bone (A) and decellularized cancellous bone (B). The scale bar indicates 100 μm.

in low glucose Dulbecco's modified Eagle's medium (Gibco, USA) supplemented with 10% fetal bovine serum (Gibco, USA) and penicillin/streptomycin. After 3 days, the culture medium was replaced for removal of nonadherent cells. When the cells grew to near confluence, they were washed with phosphate-buffered saline (PBS) and harvested from flasks by 0.25% trypsin/0.01% EDTA. These cells were subcultured when they reached 75%−85% confluence. Rat MSCs in passages 3−4 were used for the following experiments.

2.2. Preparation of Collagen/HA Composite. The HA power was fabricated from its precursors, calcium nitrate tetrahydrate $(Ca(NO_3)_2 \cdot 4H_2O$, Keshi, China) and sodium phosphate tribasic $(Na_3PO_4 \cdot 12H_2O$, Keshi, China), in our laboratory, as described previously.[28]

Pure collagen type I sponge from a bovine tendon was purchased from Shanghai Wingch Chemical Technology Co. Ltd., China. Collagen solutions at concentrations of 0.35, 0.5, or 0.7 wt % were prepared in 0.01 M HCl solution. Briefly, the collagen sponge was added into the HCl solution and stirred overnight at 4 °C. These solutions were subsequently centrifuged to remove air bubbles. Defined collagen solutions were then mixed with a calculated amount of HA powder to prepare 22 wt % mixtures of HA in the collagen solutions under constant stirring by a magnetic stirring apparatus at room temperature for 3 days.

2.3. Preparation of Decellularized Bone Scaffold. The decellularized bone scaffold was prepared by a porcine cancellous bone as previously described,[29,30] and some improvements were made. Briefly, fresh cancellous bone was harvested from the femoral head of a white swine from a local slaughterhouse (Shapingba, Chongqing, China). To reduce the difference among the different decellularized bone scaffolds, all scaffolds were taken from the same place of the femoral head. The femoral head was soaked with 0.9% saline and was immediately processed under clean conditions in the laboratory. The samples were cleaned by removing the residual tissues, sectioned into discs (10 mm in diameter and 5 mm in thickness), rinsed, and immersed in distilled water overnight at 4 °C. Then, the samples were decellularized by 1% Triton X-100 for 48 h, degreased with methane/methyl alcohol for 24 h, incubated with DNase (Sigma, USA) at 37 °C for 2 h, and then washed in PBS at room temperature under continuous shaking. These scaffolds were immersed in dehydrated alcohol for 4 h to remove the cellular remnants and then washed with a large amount of deionized water for 2 h before being dried. Finally, these scaffolds were stored at −80 °C before further applications.

2.4. Coating Collagen/HA Mixture on Decellularized Bone Scaffold. The prepared scaffolds were dipped in mixtures of different collagen/HA ratios for 6 h and shaken gently. After the collagen/HA mixture soaked evenly on the surface of scaffolds, the scaffolds were freeze-dried at −55 °C and 15 Pa by a freeze-dryer (Boyikang, Beijing) for 24 h. Finally, the scaffolds were sterilized by ^{60}Co γ irradiation (25 k Gay) (Allanace, Southwestern Radiation Research Center, The Third Military Medical University, Chongqing, China) and stored at −80 °C before further applications.

2.5. Characterization of Scaffold. *2.5.1. Histology.* The bone scaffolds were fixed in 4% paraformaldehyde at room temperature for 48 h. They were demineralized by using 12% EDTA-2Na (Sangon Biotech, China) for 4 weeks, dehydrated stepwise using ethanol, immersed in xylene, and embedded in paraffin. Paraffin was cut into 7 μm sections and then deparaffinized. The sections were stained with Mayer's hematoxylin and eosin (H-E) (Beyotime, China).

2.5.2. Microcomputed Tomography (μ-CT). The qualitative information on the decellularized bone scaffold architecture was obtained by μ-CT imaging using a microfocus X-ray CT system (Scanco medical AG vivaCT40, Switzerland). Special software μ-CT v6.1 of Scanco medical AG was used to visualize the 2D X-ray section images of the layered scaffolds. The slice increment is 10.5 μm. Isotropic slice data were obtained by the system and reconstructed into 2D images. These slice images were compiled and analyzed to render 3D images and used to investigate the interconnectivity of the pores, porosity, and distribution of pore size.

2.5.3. Scanning Electron Microscopy (SEM). Decellularized bone scaffolds were fixed in 2.5% glutaraldehyde at room temperature for 24 h. They were dehydrated in a graded series of ethanol (50%, 70%,
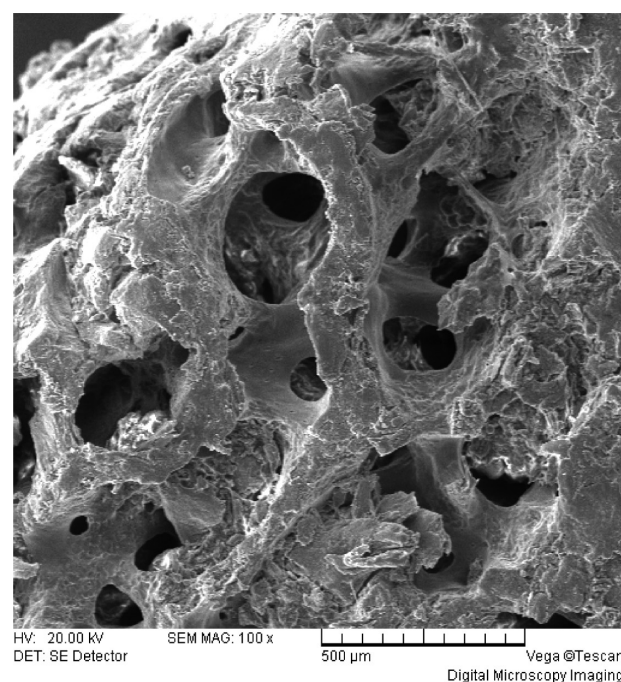

Figure 3. SEM micrographs of decellularized cancellous bone. The SEM image shows the porous structure of decellularized cancellous bone. The scale bar indicates 500 μm.
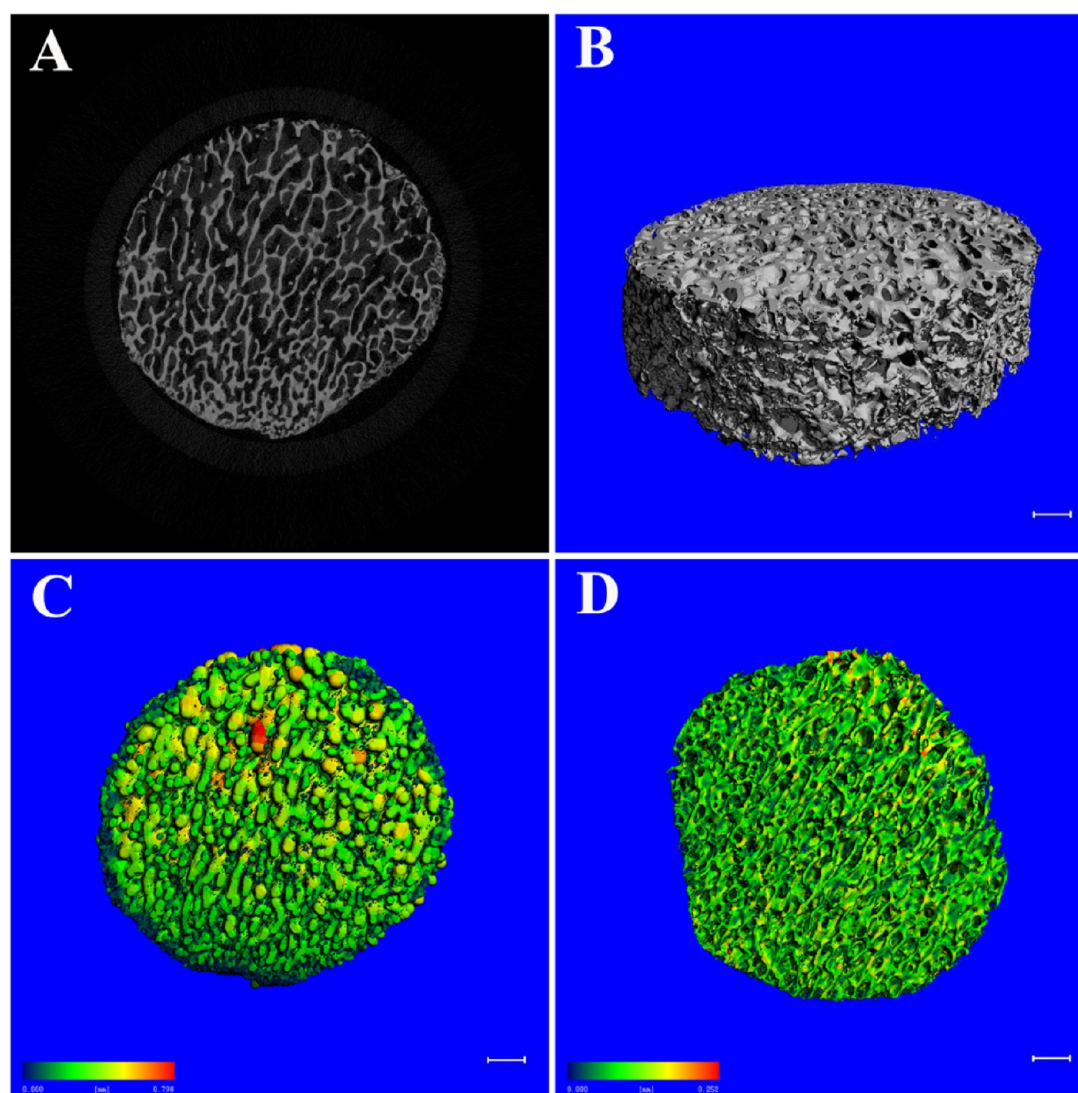
Figure 4. μ-CT images of decellularized cancellous bone scaffold. (A) 2D structure of scaffold. (B) 3D structure of scaffold. The scale bar indicates 1 mm. (C) 3D pore size distribution by μ-CT. The scale bar indicates 1 mm. (D) Wall thickness distribution by μ-CT. The scale bar indicates 1 mm.

85%, 90%, 95%, and 100%), dried at room temperature, sputter-coated with platinum for 40 s, and observed by SEM (FEI, Holland).

2.5.4. Measurement of the E of the Different Coatings on 3D Scaffolds with an Atomic Force Microscope (AFM) and Uniaxial Compression Testing. The local stiffness of different coatings on three different scaffolds was measured with an AFM (JPK, Germany) in contact mode mounted on an inverted microscope (Leica, Germany). After coating with different proportions of collagen/HA mixtures on decellularized bone scaffolds, these scaffolds were cut into sheets with 1 mm thickness. Samples were probed with a soft silicon nitride quadratic pyramid tip (0.02 N/m) (Olympus, Japan). E of the different coatings were obtained from force−indentation profiles using a Hertzian model and sample Poisson's ratio of 0.5. In such cases, we applied a force with an AFM tip at different positions along the scaffold and measured the deflection ($n \geq 20$). The force−distance curves were collected and analyzed using the JPK Imaging Process software to obtain the E of different coatings on 3D scaffolds.

The bulk stiffness of three different collagen/HA composites (cylinder: diameter = 10 mm, high = 5 mm) was measured by uniaxial compression testing ($n = 5$). All tests were carried out by using a ELF3330 mechanical testing machine (Bose, USA) which was fitted with a 22.2 N load cell. Compressive testing was performed at a strain rate of 10%/60 s. The compressive modulus was calculated in the strain range from 2% to 5% of the stress−strain curve.

2.5.5. Characterization of Collagen Type I Coated on the Scaffolds with Different Stiffness. In order to verify whether the collagen/HA mixtures have been coated on the scaffolds, the cross-sections of four groups of scaffolds were cut into 10 μm by a freezing microtome (Leica, Germany). The sections were incubated with rabbit anticollagen I antibody (Bioss, China; diluted 1:300) overnight at 4 °C in a humidified chamber. The secondary antibody was applied with an Alexa Fluor 488-labled donkey antirabbit IgG (Molecular Probes, USA; diluted 1:500). Three samples for each group were imaged by the fluorescence microscope (Olympus IX71, Japan).

2.6. Cell Seeding on Scaffold *in Vitro*. First, scaffolds were sterilized by ^{60}Co γ irradiation (25 k Gay) and then immersed in Dulbecco's modified Eagle's medium (Gibco, USA) for 2 h. Finally, scaffolds were seeded with 20 μL of cell suspension containing 4×10^5 cells. Scaffolds were flipped every 15 min for 1 h to achieve uniform cell distribution. Cell culture was maintained in an incubator at 37 °C, 5% CO_2, and 95% humidity. The medium was changed every 3 days.

2.7. Viability of Cells Seeded on Collagen/HA Decellularized Bone Scaffolds. The cell viability on decellularized bone scaffolds coated with collagen/HA was assessed by a live/dead assay. On the third day, the first week, and the third week, scaffolds were harvested and incubated in 2 μM calcein AM (staining for live cells) and 4 μM ethidium homodimer-1 (staining for dead cells) working solution for 30 min in the dark, as indicated by the manufacturer's instructions

Table 1. Composition and Property of Different Collagen/HA Scaffolds ($n = 3$)[a]

scaffold	composition		pore size (μm)		wall thickness (μm)		E (kPa)	
	collagen	HA	before coating	after coating	before coating	after coating	local	bulk
low	0.35%	22%	378.0 ± 171.7	359.8 ± 153.4	108.5 ± 36.7	113.5 ± 32.9	13.00 ± 5.55[c]	6.74 ± 1.16
medium	0.5%	22%	356.0 ± 148.3	345.7 ± 139.6	104.4 ± 37.1	114.9 ± 33.8	13.87 ± 1.51[c]	8.82 ± 2.12
high	0.7%	22%	389.3 ± 134.9	381.7 ± 152.8	107.7 ± 35.9	103.6 ± 35.4	37.70 ± 19.60[c,b]	23.61 ± 8.06[b]

[a]The local E of the control group (decellularized bone scaffold without coating) is 1.46 ± 0.44 GPa. [b]$p < 0.05$ when compared to that of the Col 0.35/HA 22 group. [c]$p < 0.05$ when compared to that of the control group.
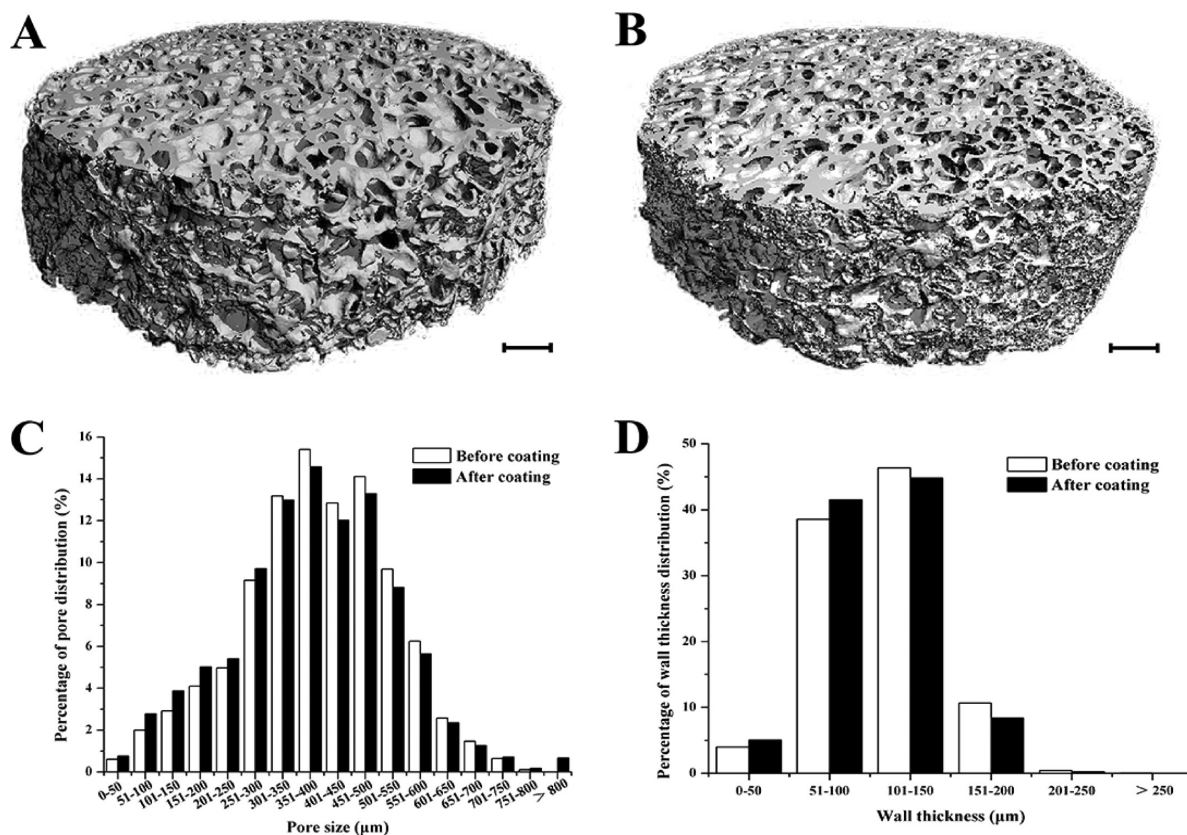

Figure 5. μ-CT images of decellularized cancellous bone scaffold before (A) and after (B) coating with the highest collagen concentration (Col 0.7/HA 22). The scale bar indicates 1 mm. (C) Pore size and (D) wall thickness distributions of decellularized cancellous bone scaffold before and after coating with the highest collagen concentration (Col 0.7/HA 22).

(LIVE/DEAD Viability/Cytotoxicity Kit, Molecular Probes, USA). After washing 3 times with PBS, the fluorescence was visualized using a fluorescence microscope (Olympus IX71, Japan).

2.8. Subcutaneous Implantation. The cylindrical-shaped scaffolds (5 mm in diameter by 4 mm in thickness) were prepared and sterilized by ^{60}Co γ irradiation (25 k Gay) before implantation. SD rats (male, body weight 230 ± 5 g) were individually housed in wire bottomed cages in a temperature- and light-controlled room. The use of rats conformed to the guiding principles in the Care and Use of Animals for our institute, and was approved by the Animal Care and Use Committee of Chongqing University. The animals were anaesthetized with 7% chloral hydrate (0.5 mL/100 g). Four of the same skin incisions were made along the dorsal midline of each rat. A decellularized bone scaffold without coating, a scaffold coated with a low-proportion of collagen (Col 0.35/HA 22), a scaffold coated with medium-proportion collagen (Col 0.5/HA 22), and a scaffold coated with high-proportion collagen (Col 0.7/HA 22) were inserted into the subcutaneous pockets at the top left corner, top right corner, bottom left corner, and bottom right corner, respectively (four animals for each time point). After 1, 3, and 6 months, rats were sacrificed, and the implanted scaffolds were removed naturally with the surrounding

tissue. Then, the samples were fixed and processed for histology as described below.

2.9. Immunohistochemistry. After culture for 14 and 21 days *in vitro* and subcutaneous implantation for 1, 3, and 6 months, samples were harvested. Each sample was fixed in 4% paraformaldehyde for 48 h at 4 °C and then decalcified with 12% EDTA-2Na (Sangon Biotech, China) for 4 weeks. Samples were dehydrated with graded ethanol washes, embedded in paraffin, and serial longitudinal sections (7 μm in thickness) prepared for histology. Paraffin sections were used for immunostaining of osteopontin (OPN) with rabbit antirat OPN polyclonal antibody (abcam, USA; diluted 1:300) or osteocalcin (OC) with rabbit antirat OC polyclonal antibody (Bioss, China; diluted 1:50). Paraffin sections were cut on a microtome and deparaffinized with xylene (twice for 15 min each). Endogenous peroxidase was inactivated with 3% hydrogen peroxide (H_2O_2) for 30 min at room temperature. The sections were incubated with a primary antibody overnight at 4 °C in a humidified chamber. The secondary antibody was applied (30 min at 37 °C), carrying horseradish peroxidase, and developed according to the manufacturer's protocol (IHC staining module, Beijing Zhongshan Biotechnology, China). Three samples for each group were analyzed by an inverted light microscope (Olympus IX71, Japan).
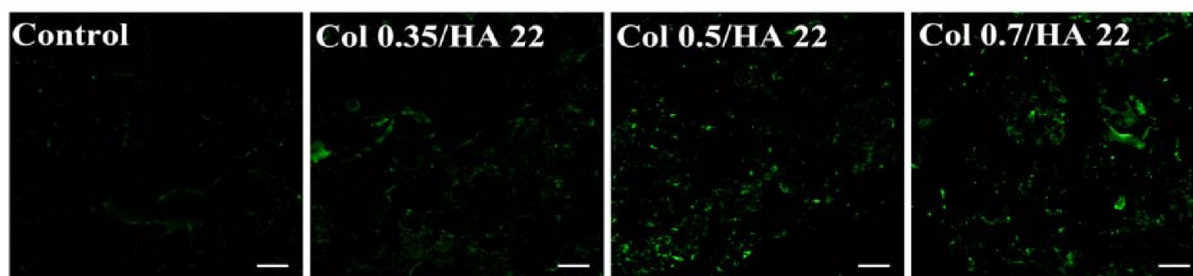
Figure 6. Immunofluorescence staining of collagen type I on the scaffolds. The green fluorescence indicates the positive staining of collagen type I. The scale bar indicates 200 μm.
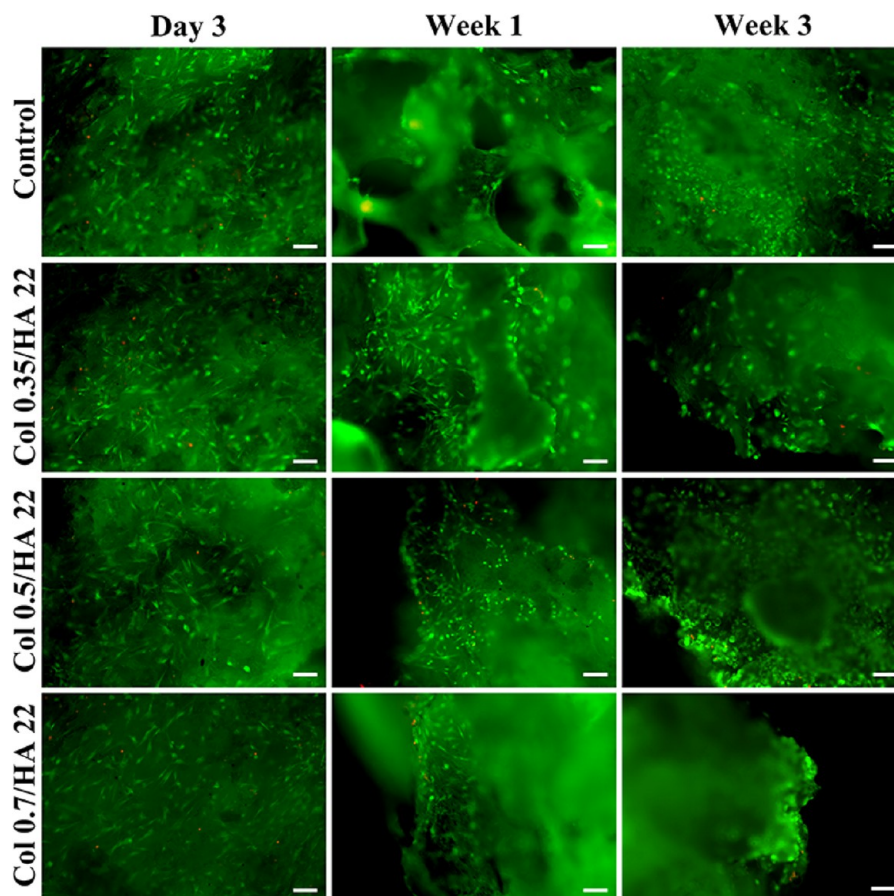

Figure 7. Live/dead assay of the scaffold along the cultivation process. Green indicates live cells, and red indicates dead cells. The scale bar indicates 100 μm.

Semiquantitative analysis of the immunohistochemical staining was analyzed using the Image-Pro Plus software. The sum of total area and integral optical density (IOD) were measured for 5 samples. The average IOD per area (IOD/area) was calculated for each group.

2.10. Immunofluorescence. After subcutaneous implantation for 1 and 6 months, samples were fixed in 4% paraformaldehyde and then decalcified in 12% EDTA-2Na for 4 weeks. The sample was cut in half, one for paraffin sections and the other for frozen sections. Frozen sections (10 μm) were then subjected to immunofluorescence for the antibody of rabbit antirat CD29, CD34, CD44, CD90, and CD105 (Bioss, China; diluted 1:300). The Alexa Fluor 488-labled donkey antirabbit IgG (Molecular Probes, USA; diluted 1:500) was used as the second antibody. DAPI (1 mg/mL) staining was used to reveal the nuclei.

2.11. Statistical Analysis. Each experiment was performed at least three times. All data are presented as the mean $\pm$ standard deviation (SD). Two group comparisons were analyzed using one-way analysis of variance (ANOVA). A p-value of less than 0.05 ($p < 0.05$) was considered to be statistically significant; * represents $p < 0.05$. All calculations were conducted using Origin 8.0 software.

3. RESULTS

3.1. Characterization of the Decellularized Bone Scaffolds. The cancellous bone was decellularized by using a process previously described.[30] These decellularized bone specimens were evaluated by histology. Staining of cell nuclei with hematoxylin shows that the nuclei were almost completely removed from the cells in bone scaffolds (Figure 2). The natural porous structure and the components of bone were well maintained in decellularized bone. Eosin staining shows that natural bone matrix in the decellularized bone was also reserved.

3.2. Architecture of the Decellularized Bone Scaffolds. SEM micrographs showing the pore architecture and trabecular
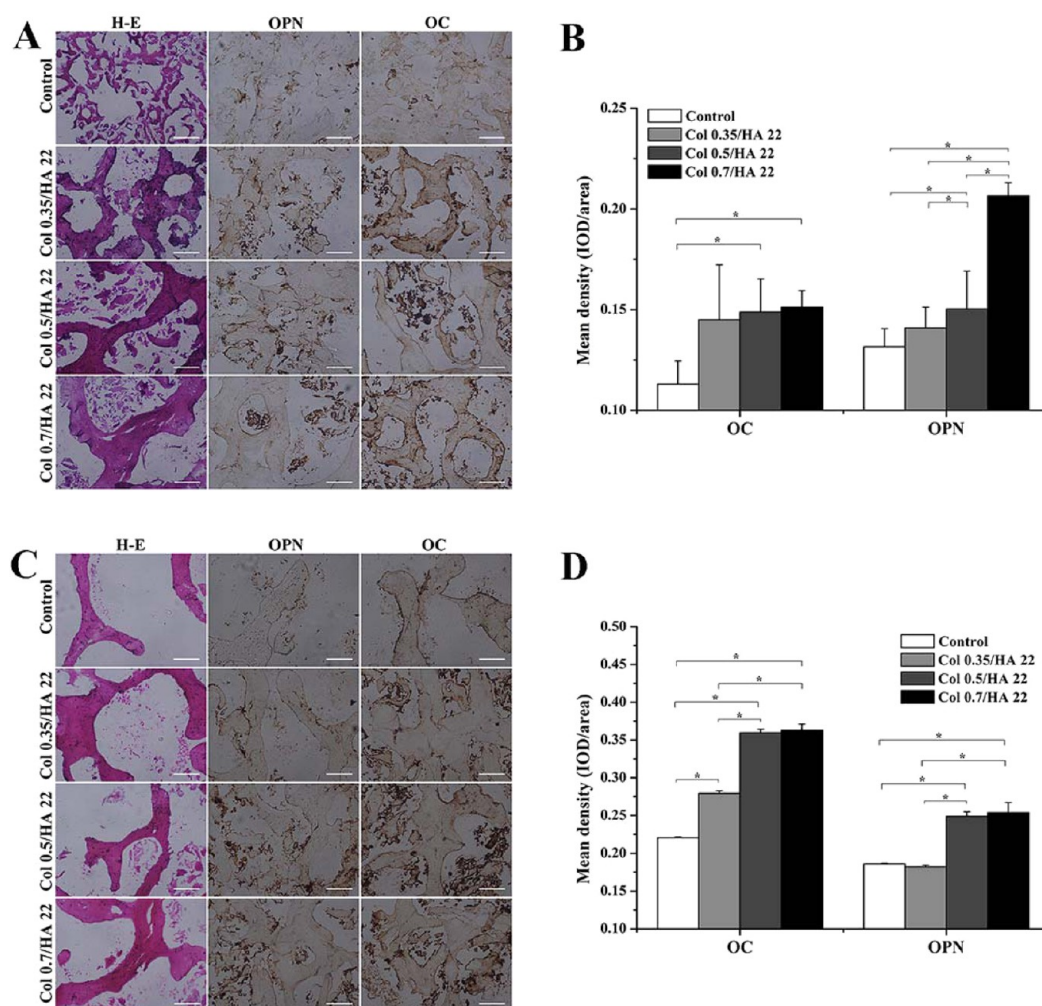
Figure 8. H-E staining and positive immunohistochemical staining of OPN and OC on scaffolds with different stiffness after culture for 14 days (A) and 21 days (C). Quantitative data for OPN and OC on scaffolds with different stiffness after culture for 14 days (B) and 21 days (D). The scale bar indicates 50 μm. * indicates $p < 0.05$.

network of the decellularized bone scaffold (Figure 3) indicate that the scaffold has good natural porous microstructure and 3D interconnectivity. Deeper insight into the pore architecture was obtained by using μ-CT, which allowed quantitative characterization of pore size, porosity, and interconnectivity. The μ-CT and 3D reconstruction image analysis of the decellularized bone clearly demonstrated the pore size distribution in 2D (Figure 4A) and the 3D interconnectivity of the porous structure (Figure 4B). From the μ-CT images, the mean pore diameter of the decellularized cancellous bone is found to be 389.3 $\pm$ 134.9 μm, and the porosity is 74.7% (Figure 4C and Table 1), and the mean wall thickness is 107.7 $\pm$ 35.9 μm (Figure 4D and Table 1).

3.3. Surface Morphology of the Scaffold and Validation of Coating. After coating with different proportions of collagen/HA mixtures on the decellularized bone scaffolds, the surface color of the scaffolds changed from faint yellow to white due to the mixture of collagen/HA formed after lyophilization. This result also implied that the collagen/HA mixture has been successfully coated on the decellularized bone scaffold. The architecture of the decellularized bone scaffolds of one sample was evaluated by μ-CT scans before and after coating with different proportions of collagen/HA mixtures (Figure 5A and B). After coating with the mixture with the

highest collagen proportion (Col 0.7/HA 22), the mean pore diameter of the scaffold was 381.7 $\pm$ 152.8 μm (Figure 5C), and the mean wall thickness was 103.6 $\pm$ 35.4 μm (Figure 5D). Before coating with this mixture (Col 0.7/HA 22), the mean pore diameter of the scaffold was 389.3 $\pm$ 134.9 μm, and the mean wall thickness was 107.7 $\pm$ 35.9 μm (Table 1). There was no statistically significant difference in the architecture of the scaffolds before or after coating ($p = 0.999$) (Table 1).

To further verify that the collagen has been successfully coated on the decellularized bone scaffold, collagen type I was detected by immunofluorescence staining (Figure 6). The results showed that collagen was successfully coated on the surface of scaffolds, and a gradient of collagen content was formed on these three coating groups. Another indirect method was used to verify whether HA has been successfully coated on the decellularized bone scaffold. A collagen/CaCO$_3$ composite was prepared and coated on the decellularized bone scaffold by the same methods previously described in the Materials and Methods section, in which HA was replaced by CaCO$_3$. In the Fourier transform infrared spectoscopy (FTIR) results (Figure S1, Supporting Information), the characteristic peak of CaCO$_3$ was shown at 720 cm^{-1}. This result also indicated that HA had been coated on the scaffold.

3.4. Mechanical Characterization of the Scaffold. The local stiffness of different coatings on 3D scaffolds was assessed
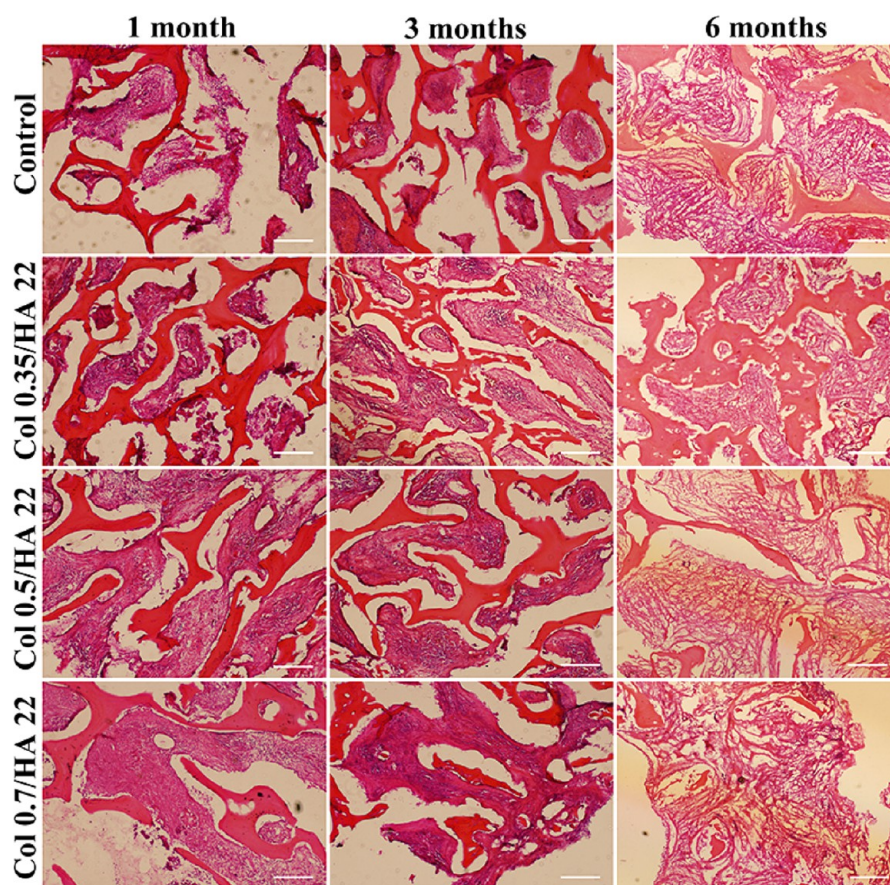
Figure 9. H-E staining of scaffolds with different stiffness scaffolds after 1, 3, and 6 months of subcutaneous implantation. The scale bar indicates 100 μm.

by AFM. The typical force versus indentation curves obtained from different scaffolds and fitted by Hertz model are shown in Figure S2 (Supporting Information). The E of the scaffold coated with a low-proportion of collagen (Col 0.35/HA 22) was 13.00 ± 5.55 kPa, while the values for medium- and high-proportions were 13.87 ± 1.51 kPa (Col 0.5/HA 22) and 37.70 ± 19.60 kPa (Col 0.7/HA 22), respectively (Table 1).

The compressive elastic modulus of collagen/HA composites with a low-proportion of collagen (Col 0.35/HA 22) was 6.74 ± 1.16 kPa, while the values for medium- and high-proportions were 8.82 ± 2.12 kPa (Col 0.5/HA 22) and 23.61 ± 8.06 kPa (Col 0.7/HA 22), respectively(Table 1). The proportion of collagen plays an important role in determining the mechanical properties of a scaffold.

3.5. Cell Compatibility of the Scaffolds with Different Stiffness. Live/dead staining can accurately distinguish live cells and dead cells (Figure S3, Supporting Information). Live/dead cell analysis revealed uniform distribution of MSCs throughout the scaffolds in periods of 3 days, 1 week, and 3 weeks, and demonstrated that most of the MSCs were viable after 3 weeks of culture with the expansion medium. MSC morphology underwent some changes in 3 weeks from spindle to round shape, especially on the Col 0.5/HA 22 scaffold (Figure 7). This result may be due to the influence of matrix stiffness on cell adhesion and spreading in 3D environment. The 3D matrix stiffness can change the integrin binding and the reorganization of adhesion ligands, both of which are traction dependent and correlated with the extent of cell adhesion and spreading. H-E staining of cultured scaffolds revealed cell infiltration and distribution after 2 and 3 weeks. In all groups,

regions close to the scaffold surface have the greatest cell density (Figure 8).

3.6. Effects of Different Stiffness on the Osteogenic Differentiation of MSCs in 3D Scaffolds. In order to evaluate the effects of different stiffness on the osteogenic differentiation of MSCs in 3D scaffolds, the expressions of two specific protein markers (OPN and OC) were examined during osteogenic differentiation. The expressions of OPN and OC evaluated by immunohistochemistry on histological sections at weeks 2 and 3 of culture showed an increase of staining in all groups over time (Figure 8A and C). After culture for 2 weeks, the positive immunohistochemical staining of OPN in Col 0.7/HA 22 is higher than that of other groups (Figure 8B). The positive immunohistochemical staining of OC exhibited a higher staining in Col 0.5/HA 22 and Col 0.7/HA 22 (Figure 8B). After culture for 3 weeks, the scaffold with the highest stiffness (Col 0.7/HA 22) exhibited significantly higher expressions of OPN and OC than the other groups, suggesting that the stiffness of 3D scaffolds significantly affects the differentiation fate of MSCs (Figure 8D).

3.7. _In Vivo_ Studies: Cell Infiltration and Immunohistochemical Staining of Bone Proteins OPN and OC. To evaluate the tissue reaction and the effects of a 3D scaffold with different matrix stiffness on the behavior and fate of host cells _in vivo_, scaffolds with different stiffness were implanted into SD rats subcutaneously. After 1, 3, and 6 months of implantation, histological sections from all groups were examined by H-E staining to detect cell infiltration (Figure 9). Figure 9 shows that cell density in the control group (decellularized bone scaffold without coating) was relatively lower than those in the
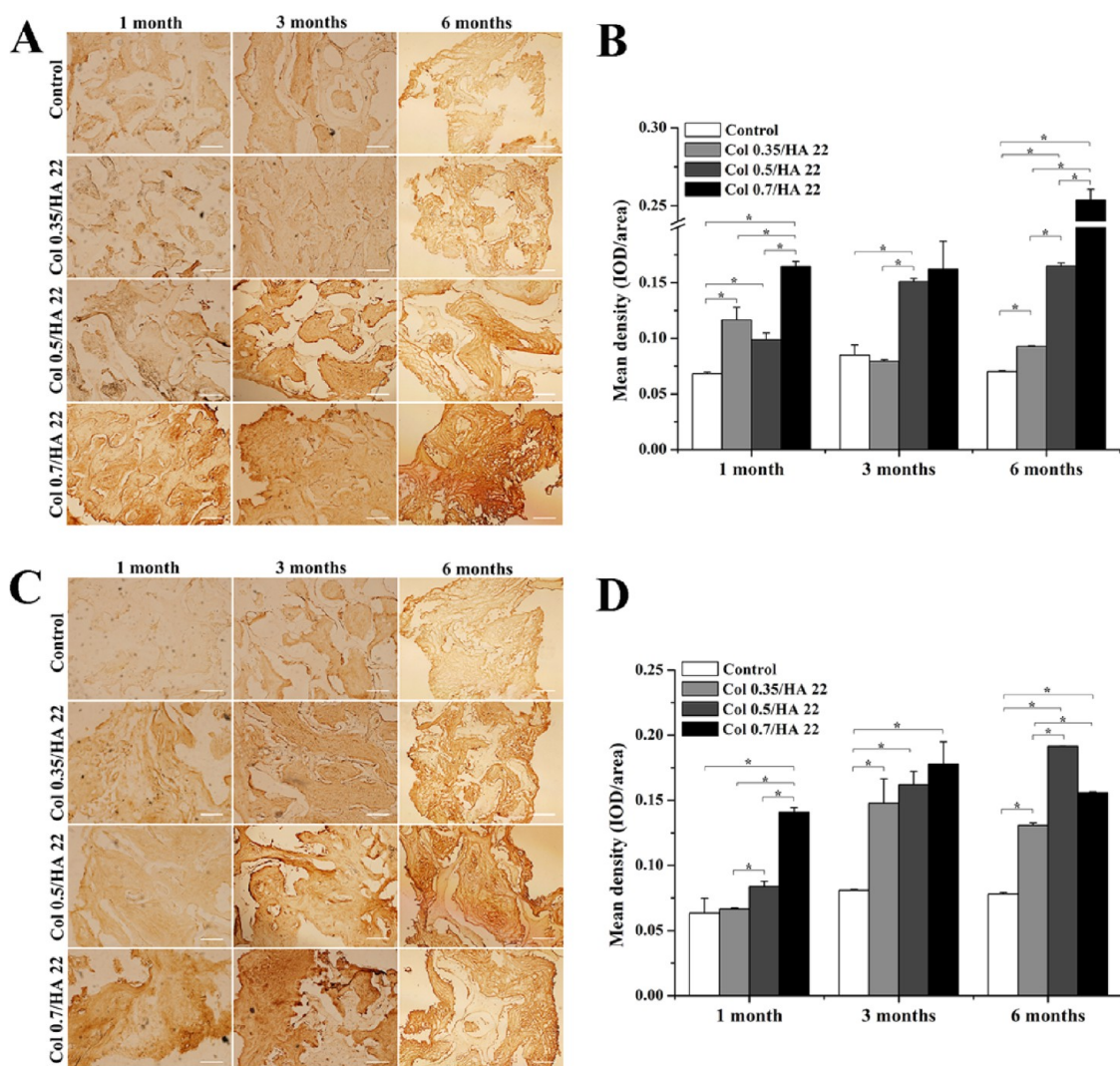
Figure 10. Immunohistochemistry staining of OPN (A) and OC (C) on scaffolds with different stiffness after 1, 3, and 6 months of subcutaneous implantation. Quantitative data for OPN (B) and OC (D) on scaffolds with different stiffness after 1, 3, and 6 months of subcutaneous implantation. The scale bar indicates 100 μm. * indicates $p < 0.05$.

coating groups after 1 month and 3 months of implantation. Cell densities in all groups after 3 months were higher than those of their corresponding groups after 1 month of implantation (Figure 9). After 6 months of implantation, cell density had no significant difference among all groups. Meanwhile, fibrous tissue was formed in each group. After the insertion of scaffolds into the subcutaneous tissue for 6 months, scaffold degradation was observed in our experiments (Figure 9). The reason for the different degradation rates of four groups of scaffolds may be due to the different numbers of invasive cells in these scaffolds. The histological results indicate that the cells infiltrated into the scaffolds and secreted their own ECM.

In addition, immunohistochemical staining of bone proteins OPN and OC was used to evaluate the fates of host cells in the scaffolds with different stiffness in 3D. After 1, 3, and 6 months of implantation, the expressions of OPN and OC gradually increased with time (Figure 10).

3.8. Utilization of Stem Cell Makers to Identify MSCs *in Vivo*. In order to identify whether there were MSCs in the implantation area, the MSC markers were tested in the present study. There were positive stainings of MSC markers CD29, CD44, CD90, and CD105 in each group of scaffold after 1 month

of implantation in subcutaneous tissue (Figure 11). The labeled positive cells migrated from the subcutaneous microenvironment to the implantation sites, making a "MSC migration flow". Immunofluorescence staining showed that the MSCs migrated *in vivo* as a cell population instead of individual cells. These results indicate that MSCs moved to the implantation area after the scaffolds were implanted for 1 month. However, the *in vivo* origin of these MSCs in rat subcutaneous tissue is still unclear.

3.9. Effects of Matrix Mechanics on Vascularization *in Vivo*. In order to evaluate the effects of matrix mechanics on vascularization *in vivo*, the expression of CD34 was detected by immunofluorescent staining after subcutaneous implantation for 6 months. CD34 is highly expressed on hematopoietic progenitors, as well as endothelial cells. In our preliminary experiments, CD34 had a very good specificity for the characterization of vascular endothelial cells in the rat carotid artery (Figure S4, Supporting Information). In Figure 12, the CD34-positive cells were detected in all four groups. The distribution of CD34-positive cells in the control group (decellularized bone scaffold without coating) was relatively random. In the other three groups, the distribution of CD34-positive cells showed varying degrees of aggregation. The typical blood
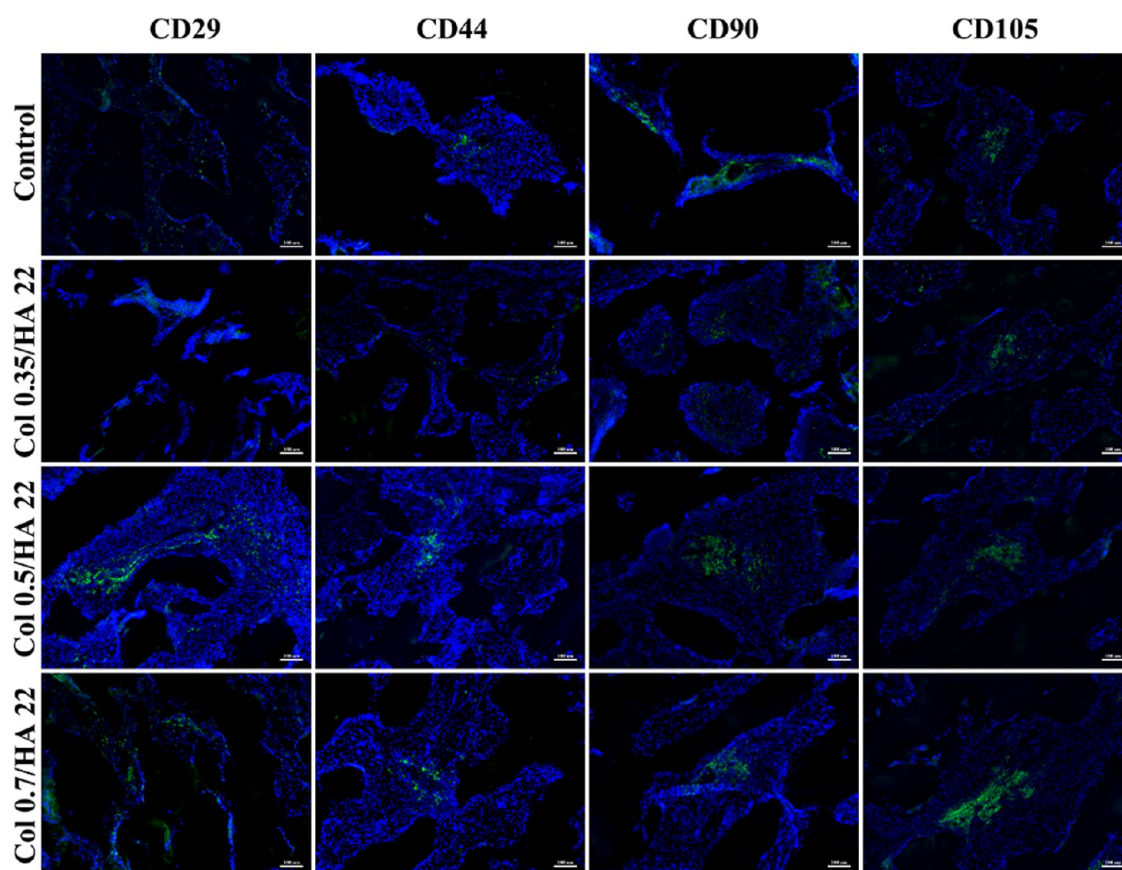
Figure 11. Immunofluorescent staining of CD29, CD44, CD90, and CD105 in the scaffold after 1 month of subcutaneous implantation. The scale bar indicates 100 μm.

vessels appeared in scaffolds coated with Col 0.5/HA 22 and scaffolds coated with Col 0.7/HA 22 (Figure 12C and D).

4. DISCUSSION

In order to study the effects of matrix mechanics on stem cell differentiation under the conditions of the real 3D environment, we have developed a new method to create 3D porous scaffolds with different stiffness while keeping the same 3D microstructures. The source of all scaffolds was from the femoral head to ensure their uniformity. Different proportions of collagen/HA mixtures were coated on the decellularized cancellous bone scaffold to create different stiffness in 3D. The decellularized cancellous bone scaffolds have a good biocompatibility, and the shape and structure can facilitate cell adhesion and proliferation. After coating of the scaffolds with different collagen/HA mixtures, examination of the viability of MSCs on the scaffolds at timed intervals showed that the collagen/HA coatings had good compatibility. After culture for 3 weeks, the MSCs on the scaffolds showed some changes in morphology; this may be due to the increase of cell density with the culture time or the occurrence of partial cell differentiation.

The pore size of the 3D scaffold is an important characteristic feature.[31] Scaffolds with a mean pore size of 325 μm have been considered to be optimal for bone tissue engineering.[32] The average pore diameter of the decellularized cancellous bone scaffold developed in our study was 389.3 $\pm$ 134.9 μm and 381.7 $\pm$ 152.8 μm before and after coating with the highest collagen proportion. This average pore size was close to the optimal pore size for cells attachment, proliferation, and migration in bone tissue engineering.

The proportion of collagen plays an important role in determining the mechanical property of the matrix.[33] To increase the matrix stiffness, the proportion of collagen in the collagen/HA mixture was increased in our experiment. As shown in Table 1, the compressive elastic modulus of collagen/HA mixtures were 6.74 $\pm$ 1.16 kPa, 8.82 $\pm$ 2.12 kPa, and 23.61 $\pm$ 8.06 kPa. After the mixtures of collagen/HA with different proportions were coated on decellularized cancellous bone, the local stiffness values were 13.00 $\pm$ 5.55 kPa, 13.87 $\pm$ 1.51 kPa, and 37.7 $\pm$ 19.6 kPa. The values of local stiffness for Col 0.35/HA 22 and Col 0.5/HA 22 groups after coating have no significant difference. Huebsch and his colleagues[21] demonstrated that the osteogenic differentiation of the MSCs occurred predominantly at 11−30 kPa, especially at 22 kPa in the 3D hydrogel. The matrix local stiffness in our experiment was set to facilitate osteogenic differentiation of MSCs. Surface coating can retain the integrity of the macroporous structure of decellularized cancellous bone, and a very thin layer was formed in the interior and exterior of the scaffold. The collagen/HA coatings in the present study can ensure no change in the microstructure of the scaffold, while the stem cells can sense the mechanical characteristics of the surface coatings.

As expected, our results revealed a strong relationship between matrix stiffness and the accumulation of bone matrix proteins, including OC and OPN. OC is a small calcium-binding protein that comprises about 10% of the total noncollagen proteins in bone and tightly adsorbs onto HA mineral surfaces. Similarly, OPN (an O-glycosylated phospo-protein) is a cell- and HA-binding protein synthesized by osteoblasts and is implicated in bone resorption.[34] Our in vitro experiments demonstrated the effects of matrix mechanics on
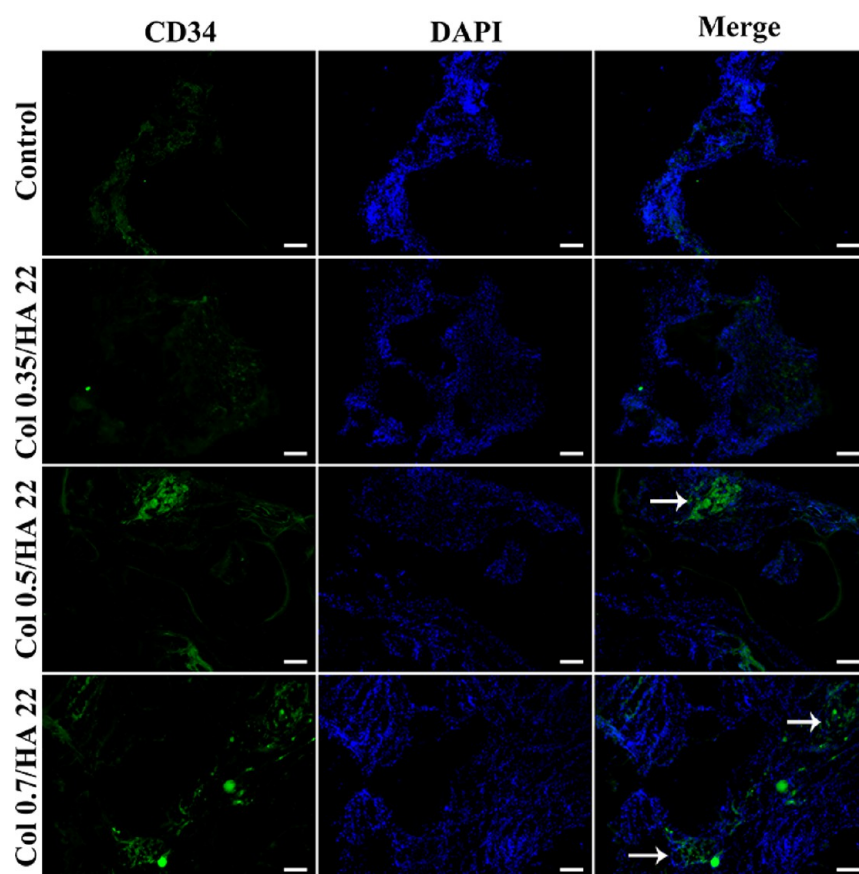
Figure 12. Immunofluorescent detection of CD34 in scaffolds with different stiffness after 6 months of subcutaneous implantation (the arrow indicates typical blood vessel). The scale bar indicates 100 μm.

the osteogenic differentiation of MSCs in 3D microenvironments. The expressions of OC and OPN on the decellularized bone scaffolds coated with collagen/HA mixtures were much higher than those in the scaffolds without coating after 2 and 3 weeks of culture. These results may be related to the surfaces stiffness of these scaffolds that the cells can feel directly. The matrix stiffness that the cell can feel and respond to should have a plateau. For example, the characteristic rigidity for NIH3T3 fibroblast cell adhesion on the scaffold surfaces has a plateau of $E > 10$ kPa. Above this approximate plateau, NIH3T3 fibroblasts show little variation in adhesion characteristic regardless of E. However, below this threshold, fibroblast cells have extraordinary sensitivity to the E value.[33] Similarly, the characteristic of cell differentiation is perhaps to have a plateau for the scaffold stiffness. In our study, the E of the control group (decellularized bone scaffold without coating) is about 1.46 ± 0.44 GPa measured by nanoindentation testing (Agilent Technologies, NANO Indenter G200, USA), which is far beyond the elasticity threshold that MSCs can sense. The elasticity range that MSCs can sense may be decided by the stiffness of the cells themselves. The present study showed that the differentiation trend of MSCs is partly consistent with the mechanical characteristics of the three scaffolds coated in vitro (Figure 8). In addition to the role of matrix stiffness, the role of collagen content in different coatings should also be considered in the experiment. Collagen type I, an ECM component of subchondral bone, is of importance for MSCs adhesion, and it may have some effect on MSC fate on the scaffolds with different matrix stiffness. Because of the very low collagen

content among the various groups, however, the effect of collagen content can be neglected.

In Figure 9, the H-E staining of histological sections of scaffolds with different stiffness demonstrated that many cells have infiltrated into the scaffolds. We hypothesize that a large number of these cells are MSCs. When the tissue or organ is damaged, the damaged part can release many "injured signals" that can recruit or mobilize MSCs to the site of injury.[35] MSCs can sense inflammation in vivo.[36] These recruited MSCs will regulate inflammatory reactions and promote tissue repair. Our experiments detected the expression of osteogenic markers OPN and OC by immunohistochemical staining to examine whether the recruited MSCs differentiate into osteoblasts. At the same time of implantation, the scaffolds coated with collagen/HA mixtures have higher OPN and OC expressions than the control group, especially at scaffolds coated with Col 0.5/HA 22 and Col 0.7/HA 22 (Figure 10). Immunofluorescent staining for MSC markers CD29, CD44, CD90, and CD105 revealed the migration of endogenous MSCs to the implantation region in all groups (Figure 11). However, we still know little about the specific origin of these MSCs that migrated into in the implantation region. Therefore, further research is needed to determine the recruitment mechanism of MSCs in vivo and the possible relationship between matrix mechanics and MSC recruitment.

One of the major challenges in the scaffold-based tissue-engineered osteogenic grafts is how to rapidly provide sufficient blood supply after implantation.[37] Vascular network formation is known to be regulated by the biophysical signals emanating from the microenvironment such as fluid shear stress.[38] Recently, Wu and his colleagues[39] seeded the human umbilical endothelial cells on scaffolds with varying stiffness to observe

the formation of capillaries. Their study revealed that cells formed well-defined networks on compliant gels (11 to 36 kPa). Further increase in hydrogel rigidity to 78 kPa reduced network assembly significantly. Interestingly, the aggregation of blood vessel-like endothelial cells appeared only in the matrices with stiffness values of 13.87 ± 1.51 kPa and 37.70 ± 19.60 kPa in our study (Figure 12C and D). Therefore, we conclude that matrix stiffness influences angiogenesis in a 3D *in vivo* environment. This may be the reason why vascular development and bone formation are tightly coupled processes during normal bone healing.[40]

In future studies, we need to better control the uniformity of the internal structure of each group of scaffolds. In addition, the static 3D culture, which does not have the provision of nutrition and removal of wastes, limits the long-term culture of stem cells or the induction of their differentiation *in vitro*. In a 3D bioreactor, perfusion and dynamic culture can overcome some limitations (cellular oxygenation, nutrition delivery, and waste removal) in static 3D culture by facilitating the exchange of oxygen and nutrients.[41] We need to investigate the effects of fluid shear force and matrix mechanics on stem cell fate.

5. CONCLUSIONS

This study has successfully constructed the 3D scaffolds with different stiffness and the same microstructure by using decellularized bone coupled with different ratios of collagen and HA. The results showed that these 3D scaffolds with different levels of stiffness can sustain the adhesion and growth of rat MSCs and promote osteogenic differentiation *in vitro*. The study also revealed that these scaffolds can recruit MSCs from subcutaneous tissue and induce them to differentiate into osteoblasts. Interestingly, these scaffolds can help angiogenesis in a 3D *in vivo* environment. The 3D scaffolds with different stiffness developed in the present study are promising cell-free scaffolds for bone tissue engineering and future clinical applications.

■ ASSOCIATED CONTENT

Ⓢ Supporting Information

Additional figures and information about the FTIR images of the decellularized bone scaffold (control) and the scaffolds coated with different proportions of collagen/HA or collagen/$CaCO_3$ mixtures; typical force versus indentation curves obtained from different scaffolds and fitted by a Hertz model; live/dead staining of live MSCs and dead MSCs; and immunofluorescent detection of CD34 in rat carotid artery. The Supporting Information is available free of charge on the ACS Publications website at DOI: 10.1021/acsami.5b02662.

■ AUTHOR INFORMATION

Corresponding Author

*Bioengineering College, Chongqing University, 174 Shazheng Jie, Shapingba, Chongqing 400044, China. Tel: 86-23-65102507. Fax: 86-23-65102507. E-mail: yglv@cqu.edu.cn.

Notes

The authors declare no competing financial interest.

■ REFERENCES

(1) Leipzig, N. D.; Shoichet, M. S. The Effect of Substrate Stiffness on Adult Neural Stem Cell Behavior. *Biomaterials* **2009**, *30*, 6867–6878.

(2) Leventhal, I.; Georges, P. C.; Janmey, P. A. Soft Biological Materials and Their Impact on Cell Function. *Soft Matter* **2007**, *3*, 299–306.

(3) Zajac, A. L.; Discher, D. E. Cell Differentiation Through Tissue Elasticity-coupled, Myosin-driven Remodeling. *Curr. Opin. Cell Biol.* **2008**, *20*, 609–615.

(4) Pajerowski, J. D.; Dahl, K. N.; Zhong, F. L.; Sammak, P. J.; Discher, D. E. Physical Plasticity of the Nucleus in Stem Cell Differentiation. *Proc. Natl. Acad. Sci. U. S. A.* **2007**, *104*, 15619–15624.

(5) McBeath, R.; Pirone, D. M.; Nelson, C. M.; Bhadriraju, K.; Chen, C. S. Cell Shape, Cytoskeleton Tension, and RhoA Regulate Stem Cell Lineage Commitment. *Dev. Cell* **2004**, *6*, 483–495.

(6) Potier, E.; Noailly, J.; Ito, K. Directing Bone Marrow-derived Stromal Cell Function with Mechanics. *J. Biomech.* **2010**, *43*, 807–817.

(7) Chowdhury, F.; Na, S.; Li, D.; Poh, Y. C.; Tanaka, T. S.; Wang, F.; Wang, N. Material Properties of the Cell Dictate Stress-induced Spreading and Differentiation in Embryonic Stem Cells. *Nat. Mater.* **2010**, *9*, 82–88.

(8) Engler, A. J.; Sen, S.; Sweeney, H. L.; Discher, D. E. Matrix Elasticity Directs Stem Cell Lineage Specification. *Cell* **2006**, *126*, 677–689.

(9) Yang, C.; Tibbitt, M. W.; Basta, L.; Anseth, K. S. Mechanical Memory and Dosing Influence Stem Cell Fate. *Nat. Mater.* **2014**, *13*, 645–652.

(10) Lee, J.; Abdeen, A. A.; Kilian, K. A. Rewiring Mesenchymal Stem Cell Lineage Specification by Switching the Biophysical Microenvironment. *Sci. Rep.* **2014**, *4*, 5188.

(11) Park, J. S.; Chu, J. S.; Tsou, A. D.; Diop, R.; Tang, Z.; Wang, A.; Li, S. The Effect of Matrix Stiffness on the Differentiation of Mesenchymal Stem Cells in Response to TGF-β. *Biomaterials* **2011**, *32*, 3921–3930.

(12) Wingate, K.; Floren, M.; Tan, Y.; Tseng, P. O.; Tan, W. Synergism of Matrix Stiffness and Vascular Endothelial Growth Factor on Mesenchymal Stem Cells for Vascular Endothelial Regeneration. *Tissue Eng., Part A* **2014**, *20*, 2503–2512.

(13) Chen, G.; Lv, Y.; Guo, P.; Lin, C.; Zhang, X.; Yang, L.; Xu, Z. Matrix Mechanics and Fluid Shear Stress Control Stem Cells Fate in Three Dimensional Microenvironment. *Curr. Stem Cell Res. Ther.* **2013**, *8*, 313–323.

(14) Lutolf, M. P.; Gilbert, P. M.; Blau, H. M. Designing Materials to Direct Stem-cell Fate. *Nature* **2009**, *462*, 433–441.

(15) Griffith, L. G.; Swartz, M. A. Capturing Complex 3D Tissue Physiology in vitro. *Nat. Rev. Mol. Cell Biol.* **2006**, *7*, 211–224.

(16) Hadjipanayi, E.; Mudera, V.; Brown, R. A. Guiding Cell Migration in 3D: A Collagen Matrix With Graded Directional Stiffness. *Cell Motil. Cytoskeleton* **2009**, *66*, 121–128.

(17) Kraehenbuehl, T. P.; Zammaretti, P.; Van der Vlies, A. J.; Schoenmakers, R. G.; Lutolf, M. P.; Jaconi, M. E.; Hubbell, J. A. Three-dimensional Extracellular Matrix-directed Cardioprogenitor Differentiation: Systematic Modulation of A Synthetic Cell-responsive PEG-hydrogel. *Biomaterials* **2008**, *29*, 2757–2766.

(18) Straley, K. S.; Heilshorn, S. C. Independent Tuning of Multiple Biomaterial Properties Using Protein Engineering. *Soft Matter* **2009**, *5*, 114–124.

(19) Levy-Mishali, M.; Zoldan, J.; Levenberg, S. Effect of Scaffold Stiffness on Myoblast Differentiation. *Tissue Eng., Part A* **2009**, *15*, 935–944.

(20) Banerjee, A.; Arha, M.; Choudhary, S.; Ashton, R. S.; Bhatia, S. R.; Schaffer, D. V.; Kane, R. S. The Influence of Hydrogel Modulus on the Proliferation and Differentiation of Encapsulated Neural Stem Cells. *Biomaterials* **2009**, *30*, 4695−4699.

(21) Huebsch, N.; Arany, P. R.; Mao, A. S.; Shvartsman, D.; Ali, O. A.; Bencherif, S. A.; Rivera-Feliciano, J.; Mooney, D. J. Harnessing Traction-mediated Manipulation of the Cell/matrix Interface to Control Stem-cell Fate. *Nat. Mater.* **2010**, *9*, 518−526.

(22) Hashimoto, Y.; Funamoto, S.; Kimura, T.; Nam, K.; Fujisato, T.; Kishida, A. The Effect of Decellularized Bone/bone marrow Produced by High-hydrostatic Pressurization on the Osteogenic Differentiation of Mesenchymal Stem Cells. *Biomaterials* **2011**, *32*, 7060−7067.

(23) Chen, Q.; Yang, Z.; Sun, S.; Huang, H.; Sun, X.; Wang, Z.; Zhang, Y.; Zhang, B. Adipose-derived Stem Cells Modified Genetically in vivo Promote Reconstruction of Bone Defects. *Cytotherapy* **2010**, *12*, 831−840.

(24) Rodrigues, C. V.; Serricella, P.; Linhares, A. B.; Guerdes, R. M.; Borojevic, R.; Rossi, M. A.; Duarte, M. E.; Farina, M. Characterization of A Bovine Collagen-hydroxyapatite Composite Scaffold for Bone Tissue Engineering. *Biomaterials* **2003**, *24*, 4987−4997.

(25) Glowacki, J.; Mizuno, S. Collagen Scaffolds for Tissue Engineering. *Biopolymers* **2008**, *89*, 338−344.

(26) Prosecká, E.; Rampichová, M.; Vojtová, L.; Tvrdík, D.; Melčáková, S.; Juhasová, J.; Plencner, M.; Jakubová, R.; Jančář, J.; Nečas, A.; Kochová, P.; Klepáček, J.; Tonar, Z.; Amler, E. Optimized Conditions for Mesenchymal Stem Cells to Differentiate into Osteoblasts on A Collagen/hydroxyapatite Matrix. *J. Biomed. Mater. Res., Part A* **2011**, *99*, 307−315.

(27) Huang, Y.; Jia, X.; Bai, K.; Gong, X.; Fan, Y. Effect of Fluid Shear Stress on Cardiomyogenic Differentiation of Rat Bone Marrow Mesenchymal Stem Cells. *Arch. Med. Res.* **2010**, *41*, 497−505.

(28) Chen, G.; Lv, Y.; Dong, C.; Yang, L. Effect of Internal Structure of Collagen/hydroxyapatite Scaffold on the Osteogenic Differentiation of Mesenchymal Stem Cells. *Curr. Stem Cell Res. Ther.* **2015**, *10*, 99−108.

(29) Sun, X. J.; Peng, W.; Yang, Z. L.; Ren, M. L.; Zhang, S. C.; Zhang, W. G.; Zhang, L. Y.; Xiao, K.; Wang, Z. G.; Zhang, B.; Wang, J. Heparin-chitosan-coated Acellular Bone Matrix Enhances Perfusion of Blood and Vascularization in Bone Tissue Engineering Scaffolds. *Tissue Eng., Part A* **2011**, *17*, 2369−2378.

(30) Marcos-Campos, I.; Marolt, D.; Petridis, P.; Bhumiratana, S.; Schmidt, D.; Vunjak-Novakovic, G. Bone Scaffold Architecture Modulates the Development of Mineralized Bone Matrix by Human Embryonic Stem Cells. *Biomaterials* **2012**, *33*, 8329−8342.

(31) Hofmann, S.; Hagenmüller, H.; Koch, A. M.; Müller, R.; Vunjak-Novakovic, G.; Kaplan, D. L.; Merkle, H. P.; Meinel, L. Control of in vitro Tissue-engineered Bone-like Structures Using Human Mesenchymal Stem Cells and Porous Silk Scaffolds. *Biomaterials* **2007**, *28*, 1152−1162.

(32) Murphy, C. M.; Haugh, M. G.; O'Brien, F. J. The Effect of Mean Pore Size on Cell Attachment, Proliferation and Migration in Collagen-glycosaminoglycan Scaffolds for Bone Tissue Engineering. *Biomaterials* **2010**, *31*, 461−466.

(33) Saxena, S.; Spears, M. W., Jr.; Yoshida, H.; Gaulding, J. C.; García, A. J.; Lyon, L. A. Microgel Film Dynamics Modulate Cell Adhesion Behavior. *Soft Matter* **2014**, *10*, 1356−1364.

(34) Shah, N. J.; Hong, J.; Hyder, M. N.; Hammond, P. T. Osteophilic Multilayer Coatings for Accelerated Bone Tissue Growth. *Adv. Mater.* **2012**, *24*, 1445−1450.

(35) Yellowley, C. CXCL12/CXCR4 Signaling and Other Recruitment and Homing Pathways in Fracture Repair. *BoneKEy Rep.* **2013**, *2*, 300.

(36) Bernardo, M. E.; Fibbe, W. E. Mesenchymal Stromal Cells: Sensors and Switchers of Inflammation. *Cell Stem Cell.* **2013**, *13*, 392−402.

(37) Mercado-Pagán, Á. E.; Stahl, A. M.; Shanjani, Y.; Yang, Y. Vascularization in Bone Tissue Engineering Constructs. *Ann. Biomed. Eng.* **2015**, *43*, 718−729.

(38) Zhang, C.; Zeng, L.; Emanueli, C.; Xu, Q. Blood Flow and Stem Cells in Vascular Disease. *Cardiovasc. Res.* **2013**, *99*, 251−259.

(39) Wu, Y.; Al-Ameen, M. A.; Ghosh, G. Integrated Effects of Matrix Mechanics and Vascular Endothelial Growth Factor (VEGF) on Capillary Sprouting. *Ann. Biomed. Eng.* **2014**, *42*, 1024−1036.

(40) Hutton, D. L.; Grayson, W. L. Stem Cell-based Approaches to Engineering Vascularized Bone. *Curr. Opin. Chem. Eng.* **2014**, *3*, 75−82.

(41) Kraehenbuehl, T. P.; Langer, R.; Ferreira, L. S. Three-dimensional Biomaterials for the Study of Human Pluripotent Stem Cells. *Nat. Methods* **2011**, *8*, 731−736.